IEEE Access
Multidisciplinary | Rapid Review | Open Access Journal

Received November 4, 2020, accepted November 26, 2020, date of publication December 7, 2020,
date of current version December 18, 2020.

Digital Object Identifier 10.1109/ACCESS.2020.3042795

Group Connectivity-Based UAV Positioning and Data Slot Allocation for Tactical MANET

JAE SEANG LEE[1], (Member, IEEE), YOON-SIK YOO[2], (Member, IEEE), HYUNGSEOK CHOI[1], TAEJOON KIM[3,4], (Member, IEEE), AND JUN KYUN CHOI[5], (Senior Member, IEEE)

[1]Agency for Defense Development, Daejeon 34199, South Korea
[2]Electronics and Telecommunications Research Institute, Daejeon 34129, South Korea
[3]School of Information and Communications Engineering, Chungbuk National University, Chungju 28644, South Korea
[4]Research Institute for Computer and Information Communication, Chungbuk National University, Chungju 28644, South Korea
[5]School of Electrical Engineering, KAIST, Daejeon 34141, South Korea

Corresponding author: Taejoon Kim (ktjcc@chungbuk.ac.kr)

This work was supported by the Agency for Defense Development and Defense Acquisition Program Administration through the Small-Scale Mobile Ad-Hoc Network With Bio-Networking Technology Project under Grant ADD-912583201.

ABSTRACT On a future tactical-battle field network, combat radio nodes will be deployed for various operations, forming a mobile ad-hoc network (MANET). However, because of the nodes' mobility, a single group might be divided into several small groups with fewer nodes. Conversely, several small groups might be merged into one group. In such an environment, an unmanned aerial vehicle (UAV) will provide an effective way to improve network coverage and connectivity among the small groups. However, some issues should be considered for the optimal deployment of the UAV. One issue is to find the proper position of the UAV, which enhances the connectivity among the groups, because a tactical network places a high priority on network survivability rather than throughput maximization. We also need to exploit real topographic information to obtain more accurate connectivity information among nodes. Second, an efficient resource allocation scheme for reliable communications through the UAV should be taken into account. Since most of the links between the UAV and the ground nodes are line-of-sight (LoS), due to the good quality of these links, the traffic via the UAV will be heavy in spite of the limited data slot resources. Moreover, the traffic flows of the network require diverse quality-of-service (QoS), and different priorities should be imposed upon the nodes depending on the involved tactical operations. In this paper, we formulate a UAV positioning problem maximizing group connectivity (GC) and a data slot-allocation problem maximizing GC utility. Subsequently, we propose an optimal positioning and slot allocation algorithm, which satisfies QoS requirement and supports the predetermined priorities of the nodes and the groups. Numerical analysis verifies that the proposed scheme is effective in UAV positioning and slot allocation, outperforming conventional methods.

INDEX TERMS Tactical mobile ad-hoc network, unmanned aerial vehicle, positioning, data slot allocation.

I. INTRODUCTION

On a future tactical-battle field network, combat radio nodes will be deployed, forming a mobile ad-hoc network (MANET) without intervention from a central base station [1]. However, diverse battle-field operations will require a flexible formation of the network. A single group, in which nodes can communicate with the other nodes using ground ad-hoc networking, might be divided into several smaller groups with fewer nodes. Or several small groups might be merged into one. Moreover, tactical environments and requirements, such as an operation on mountainous terrain, and a real-time transmission requirement are challenging issues for a tactical MANET as illustrated in Fig. 1.

In this environment, an unmanned aerial vehicle (UAV) can be an effective alternative to enlarge coverage and increase connectivity among small groups. However, some issues should be considered for the optimal deployment of the UAV. The first one is to find the proper position of the UAV that enhances inter-group connectivity. In a commercial network, maximization of throughput or the number of users to be served are main concerns, whereas in a tactical MANET, maintaining inter-group connections for the survivability of the network is more important. Note that even if only a single

The associate editor coordinating the review of this manuscript and approving it for publication was Maurizio Magarini.

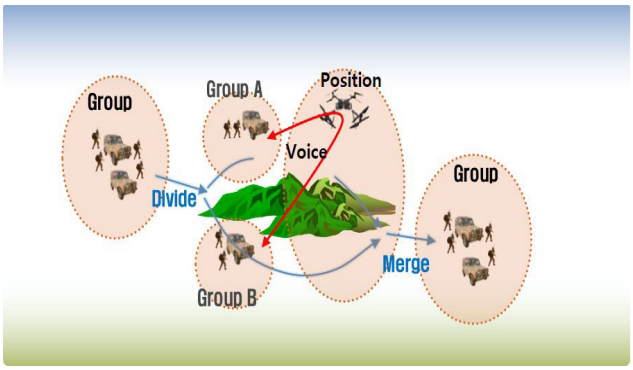

FIGURE 1. Network group operations and the environment in a tactical MANET.

node in a group is connected to a UAV, the remaining nodes of the group can communicate with the other groups via the UAV as long as the intra-group connections are secured.

Second, an efficient resource allocation scheme for reliable communications via the UAV is required. Although a tactical MANET has a limited number of data slots, many nodes can connect to the UAV through line-of-sight (LoS) links. Hence, a UAV with good link quality will be congested with heavy traffic to and from ground nodes. In addition, there are diverse quality-of-service (QoS) requirements according to various types of traffic, such as urgent messages and real-time voice traffic, or simple status report messages. Moreover, there are different priorities according to the nodes' ranks and the importance of the groups associated with the tactical operations imposed upon them.

In [2]–[11], studies to find the proper position of a UAV were mainly focusing on commercial communications. In [2], a UAV was used to increase coverage of a network and to provide a remedy for unexpected incidents, such as urgent communications. In [3] and [4], the authors showed that a UAV is an effective solution for overcoming ground station failures by providing service to remote users and improving QoS. In [5], a path loss model for communication between a UAV and a ground user was proposed, and this model was adopted to obtain the optimal altitude of a UAV, which maximizes the coverage of a network. In [6], 3D deployment of a UAV was examined to serve as many nodes as possible. In [7], to increase network capacity, the authors proposed a method to connect mobile-communications cell areas with a UAV. Additionally, the deployment of multiple UAVs was investigated to provide non-overlapping coverage areas and to enhance link capacity for ground nodes in hotspot areas. Specifically, efficient placement of a UAV was obtained using the circle packing theory. In [8], the optimal altitude for a UAV was determined for a guaranteed reliability factor considering a single node at the cell edge. In [9], the authors proposed a UAV placement strategy in 2D to minimize average latency for a heterogeneous network (HetNet). In [10], 3D placement of a UAV in a hotspot was studied. The goal was to maximize the number of nodes the UAV can cover, and the proposed scheme introduced different QoS constraints. In [11], node selection and power allocation problems were investigated to maximize network utilities in multiple small-cell networks.

The foremost difference between our work and those studies is that the other studies did not consider scenarios where a network of a single group is divided as the group moves. When a UAV can connect small divided groups, linking the separate groups is much more important than increasing the number of nodes directly covered by the UAV. Therefore, in order to support more than two groups, the position of the UAV should be decided considering inter-group connectivity. Instead of just the number of nodes to be connected, the connectivity among the groups reflecting the topology of the network is taken into account. Moreover, the other studies did not consider the geographic environment. Obstacles such as mountainous areas in tactical environments are major limiting factors to communication, and consequently, terrain information must be reflected. The difference from other algorithms is that the connectivity is obtained using topographic information, and hence, more accurate connectivity information can be obtained.

There are various studies on media access control (MAC) protocols providing QoS for a MANET. The majority of them can be categorized into contention-based carrier sense multiple access (CSMA), contention-free time division multiple access (TDMA), or a hybrid of the two, as discussed in [12] and [13]. TDMA is effective in transmitting real-time data, guaranteeing QoS in a tactical MANET [1]. Accordingly, tactical radio [14] is adopting this access scheme, and dynamic slot allocation based on user demand was investigated in [15]–[21]. In [15], multi-hop desynchronization (MH-Desync) was proposed, where each node exchanges slot information with its own one-hop neighboring nodes to allocate unused slots. Accordingly, through exchanging this information, each node can obtain its 2-hop nodes slot allocation information. In [16], Kuramoto-Desynchronization (K-Desync) was proposed for a rapid convergence of desynchronization. In [17], weight desynchronization (W-Desync) was proposed, and QoS was considered by assigning weight factors. In [1], a QoS-attaining scheme considering energy efficiency was proposed. In [18], a TDMA-based multihop resource reservation (TMRR) scheme was proposed for flow-based slot scheduling in order to minimize end-to-end delay, and the slot information in a beacon slot is exchanged in every frame. In [19], a contention-based slot allocation scheme, that reflects topology changes and traffic demand, was proposed. In [20], 1-hop node information was exchanged among nodes, and slots were scheduled according to the required number of slots. In [21], a distributed TDMA protocol was proposed considering on-demand frame size. In [22]–[25], MAC protocols guaranteeing minimum slot allocation to every node have been proposed. In [22], the authors proposed a distributed slot allocation protocol that supports multi-hop connections. In [23], the authors proposed a five-phase reservation protocol (FPRP), where contention-based slot allocation was adopted. In [24], the authors proposed

a distributed randomized time slot assignment algorithm, called DRAND, which schedules slots based on contention by exchanging 1-hop node information. In [25], the authors proposed a scheduling policy based on unused slot information exchanged among 1-hop nodes. However, the above-mentioned protocols do not consider slot allocation when the total number of slots is less than the sum of the requested slots. When the sum of the requested slots is greater than the number of available slots, a slot allocation policy for a UAV is required, and the importance of the nodes and of the traffic types traversing the UAV are important factors in designing the policy. For high reliability and survivability of the MANET, QoS and real-time transmission capability are important factors. QoS and the importance of the traffic should be determined based on the characteristics of the traffic and on whether the traffic traverses via the UAV or not. Traffic that traverses through separate groups is more important than intra-group traffic because, for intra-group traffic, there can be many alternative paths through substitute ground links.

The main contributions of this work are fourfold.

- We define new group connectivity (GC) considering the numbers of linked nodes and linked groups. For a tactical environment, geographic information is considered in checking link availability.
- We propose a UAV positioning mechanism that maximizes group connectivity. When there is a single group, we search the optimal UAV position for maximizing the number of nodes that can establish a connection with the UAV. On the other hand, with more than two groups, inter-group connection via the UAV is the most important factor in finding the optimal position.
- We define a new GC utility, which combines a normalized QoS satisfaction function and a group weight function.
- We propose a dynamic data slot allocation mechanism for maximizing the GC utility.

The rest of this paper is organized as follows. In Section II, the system model and problem formulations are presented. The proposed algorithms are described in Section III, followed by a detailed presentation of the numerical results and a related discussion in Section IV. Finally, conclusions are drawn in Section V.

II. SYSTEM MODEL AND PROBLEM FORMULATIONS

A. SYSTEM MODEL

1) AIR-TO-GROUND CHANNEL MODELS

There are various channel effects associated with air-to-ground link budgets such as path loss, shadowing, multipath fading, atmospheric loss, and rain fading [26]. In [27]–[31], the free-space model is applied to the path loss, and other channel effects are added for link budgets.

Instead of a free-space pathloss model, we adopt the military Terrain Integrated Rough Earth Model 4 (TIREM-4) [32] in order to consider geographic effects in a tactical environment. The terrain information determines whether LoS/NLoS, reflection, and diffraction of signals are to be applied or not. In Fig. 2, the lower sub-figure represents terrain information, and the upper sub-figure shows the signal attenuation between the two points in the terrain information. As shown in the upper sub-figure, the propagation diffraction is applied when the LoS is interrupted by the terrain elevation on the path. Digital Terrain Elevation Data 2 (DTED-2) [33] format is used as the terrain information for the TIREM-4 model. Shadowing and atmospheric loss effects are also applied in TIREM-4, and, considering these effects together, a more accurate channel path loss model can be obtained when the operation area is determined. As a multipath fading model, Rician distribution [34] is applied, and the available frequency band determines the K factor of this distribution [35]. Since an air node might operate in rainy or snowy conditions, the rainfall reduction model defined in the ITU-R P.618-13 standard [36] is adopted. This model is applied between 1 GHz and 1000 GHz center frequencies, but there is little rainfall attenuation in the vicinity of the 1 GHz band, and it gradually increases with frequency; hence, it is assumed that rainfall attenuation does not occur below 1 GHz. The applied models are summarized in Table 1.

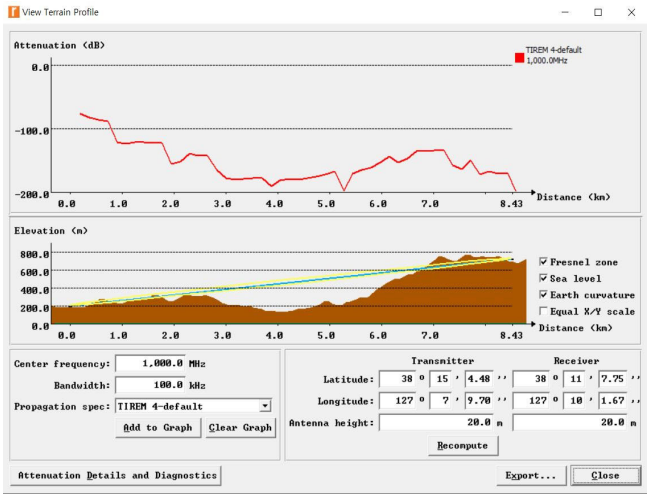

FIGURE 2. The TIREM-4 model.

TABLE 1. Channel Characteristics and Applied Models.

Channel Characteristics	Applied Model
Path loss	TIREM-4
Shadowing	TIREM-4
Multipath fading	Rician Distribution
Atmospheric loss	TIREM-4
Rain fading	ITU-R P.618-13

The received power at node i from a transmitter with power P_t, called Effective Isotropic Radiated Power (EIRP), can be expressed as

$$P_r = P_t - Loss_{TIREM}(h, r_i) - Loss_{Rician} - Loss_{Rain}, \quad (1)$$

where h and r_i are the vertical distance from the ground and the horizontal distance from ground node i, respectively. The received power should exceed a certain threshold, P_{th}, which

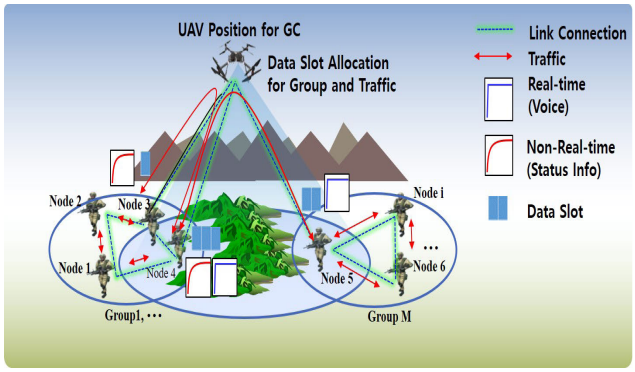

FIGURE 3. Proposed GC-TMAC system model.

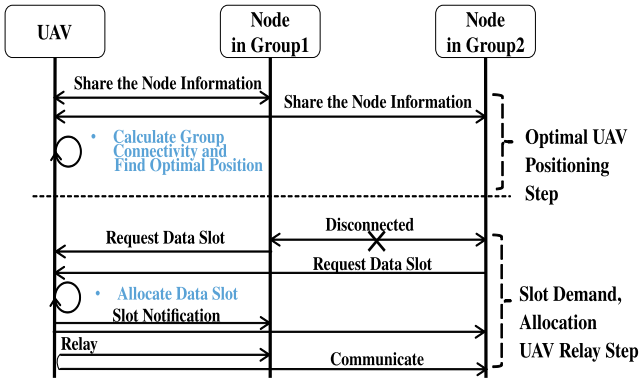

FIGURE 4. The UAV positioning step, and the relay step.

is the design parameter that refers to equipment performance, to guarantee an active communications link. Accordingly, attenuation on the communications link must be less than a certain level of channel loss.

2) SYSTEM AND QOS SATISFACTION MODELS

The Group Connectivity Tactical Medium Access Control (GC-TMAC) system is described in Fig. 3, where a UAV can support a single group or multiple divided groups. Ground nodes of a group are interconnected in an ad-hoc mode, and the UAV supports communications among the ground nodes. Ground nodes usually send real-time voice data or non-real-time status information.

A schematic of the operational flow is given in Fig. 4. First, each node shares node information with the UAV as well as its neighbor nodes. The UAV searches for the optimal position and moves there. If communication between the groups is cut off, one node of each group requests a data slot to the UAV. Then, the UAV executes a slot allocation algorithm, and the allocation information is delivered to the ground nodes. The UAV constantly checks the neighbor information of the network. The location of the UAV is periodically updated, and the period is determined according to the speed of the ground nodes, the link state, and the connectivity among the nodes. We assume that a ground node is carried by a human, and the location of the UAV node is updated once every T_p, which is the UAV position update period. In the numerical results, T_p is set to 5 minutes because it is assumed that infantry soldiers carry the ground nodes.

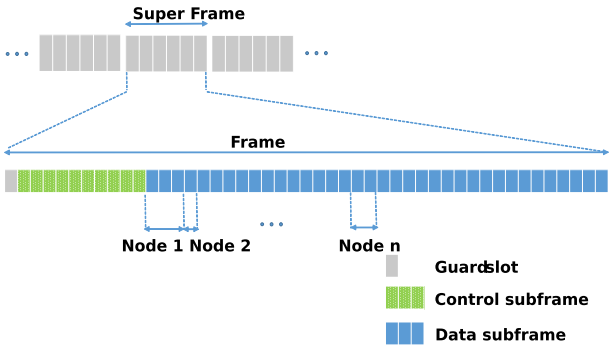

FIGURE 5. The TDMA superframe structure of the proposed GC-TMAC.

There are two different types of subframe constituting a superframe of the system (the *Control subframe* and the *Data subframe*) as shown in Fig. 5. Using the *Control Slot* in the *Control subframe*, each node sends its NCF (Network ConFiguration) message to make a connection with other nodes including the UAV. In addition, each node sends slot requests, neighbor node information, and node status reports to the UAV using the *Control Slot*. Moreover, the UAV sends the slot scheduling information to the ground nodes using the *Control Slot*. The status of 1-hop neighbors for each node is also shared using the *Control Slot*. If the total number of slot requests is smaller than the total number of unused slots in the UAV, the slots are assigned upon request. On the other hand, if the total number of slot requests is greater than the total number of unused slots (that is, if it is a saturated network), then a slot assignment policy is required. In connection establishment and packet routing, all the nodes are operating in an ad-hoc mode that supports a maximum 4-hop communication. The number of hops is related to the operation area of the nodes, the superframe size, and the traffic delay requirement. The maximum hops is determined by the operation area of the nodes, and the superframe size is designed to accommodate the maximum hops because the end-to-end delay increases as the number of hops increases. If a node fails to receive a data slot allocation, it tries again; however, in case of consecutive failures, the routing path is reset in the upper layer.

In Eq. (2), QoS satisfaction function $Q_i(s_i)$ is defined, and functions of this type are widely used to model the characteristics of networks. In particular, because real-time data are inelastic and delay-sensitive, a QoS satisfaction model can be presented in the form of S-shapes, and the standardized utility features are available. On the other hand, as non-real-time data are elastic and delay-tolerant, a QoS satisfaction model can be an incremental function [37].

$$Q_i(s_i) = \begin{cases} c_i \left(\dfrac{1}{1+\exp(-a_i(s_i-b_i))} - d_i \right), & \text{if real-time,} \\ \dfrac{\log(1+k_i s_i)}{\log(1+k_i s_{max})}, & \text{if non-real-time,} \end{cases} \tag{2}$$

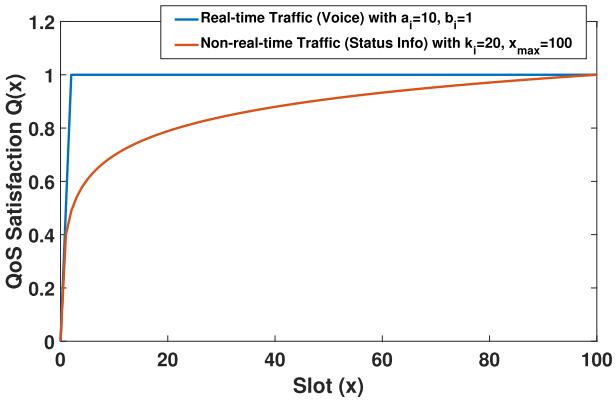

FIGURE 6. QoS satisfaction functions of the proposed GC-TMAC.

In Eq. (2), s_i is the number of slots allocated to node i: a_i, b_i, k_i, and s_{max} are parameters to be adjusted, and $c_i = \frac{1+\exp(a_i b_i)}{\exp(a_i b_i)}$, $d_i = \frac{1}{1+\exp(a_i b_i)}$, $Q_i(\infty) = 1$, and $Q_i(0) = 0$. As shown in Fig. 6, the blue and red graph lines, respectively, indicate QoS satisfaction for real-time voice traffic and non-real-time traffic (such as status information). For real-time traffic, such as voice data, the packet size is small, and accordingly, the satisfaction level increases to 1 immediately after a single slot is allocated. In other words, satisfaction is determined by whether slots are assigned or not. This satisfaction level does not increase further, even when more slots are allocated to voice traffic. It is assumed that the MELPe 2.4k military standard codec [38] is used, and traffic delay is within 225 ms per hop. That is, the QoS level is fully saturated if slot allocation supports only 2.4 kbps. Therefore, the QoS level will be binary, representing whether the call quality required to make a voice call is satisfied or not, so that voice calls can be made, which can make the blue satisfaction curve in Fig. 6. The red graph line shows the logarithmic shape function representing the QoS level of delay-tolerant and non-real-time traffic [39]. We assume the delay requirement for data traffic is loose.

B. PROBLEM FORMULATIONS

1) UAV POSITIONING PROBLEM

In this subsection, a UAV positioning problem is presented considering group connectivity. The optimal UAV position will be dependent on the performance metric (index) adopted. In this paper, two metrics (node connectivity and inter-group connectivity) are considered. Node connectivity is the number of nodes that are able to establish a connection to the UAV. It means that the link path loss between the node and the UAV is less than the loss threshold, $Loss_{max}$. Inter-group connectivity is the number of groups that are directly linked to the UAV. A group is declared to be directly linked to the UAV if at least a single node of the group is directly linked to the UAV. For the purpose of maintaining network survivability, the link connectivity between two nodes that belong to different groups plays an important role. Hence, we define group connectivity using two metrics conjointly. Group connectivity based on the UAV position (x_u, y_u, h_u) is defined as

$$C_{\text{group}}(x_u, y_u, h_u) = \sum_{i\in\mathcal{N}} \alpha_i I_i(x_u, y_u, h_u) + \sum_{j\in\mathcal{M}} \beta_j G_j(x_u, y_u, h_u), \quad (3)$$

where α_i and β_j are the priority of node i and the weight of group j, respectively. $\mathcal{N} = \{1, 2, \ldots, N\}$ and $\mathcal{M} = \{1, 2, \ldots, M\}$ are the indexing sets of the nodes and the groups, respectively, and $0 \le \alpha_i \le 1$, $\beta_j \ge 1$, and $I_i(x_u, y_u, h_u)$ and $G_j(x_u, y_u, h_u)$ are indicator functions defined as follows:

$$I_i(x_u, y_u, h_u) = \begin{cases} 1, & \text{if } P_{r_i} \ge P_{th} \\ 0, & \text{otherwise.} \end{cases}$$

$$G_j(x_u, y_u, h_u) = \begin{cases} 1, & \text{if } P_{r_j} \ge P_{th} \\ 0, & \text{otherwise.} \end{cases}$$

where P_{r_i}, and P_{th}, respectively, are received power of the UAV from ground node i in Eq. (1), and the power threshold to guarantee an active communications link. As explained in Section II, we adopt the TIREM-4 model to take geographic effects in a tactical environment into account. From this model, the signal attenuation and received power between node i and the UAV can be calculated. We assume that the j-th group is connected to the UAV when at least one node in the j-th group is connected to the UAV.

We can formulate the group connectivity optimization problem based on (3).

Problem 1: Group Connectivity Optimization

$$\begin{aligned} \max_{Z} \ & C_{\text{group}}(x_u, y_u, h_u) \\ s.t. \ & C1 : x_{\min} \le x_u \le x_{\max} \\ & C2 : y_{\min} \le y_u \le y_{\max} \\ & C3 : h_{\min} \le h_u \le h_{\max} \\ & C4 : I_i \in \{0, 1\}, i \in \mathcal{N} \\ & C5 : G_j \in \{0, 1\}, j \in \mathcal{M}, \end{aligned} \quad (4)$$

where $Z = [x_u, y_u, h_u]^\intercal$ represents UAV 3D coordinates, in which $[\cdot]^\intercal$ is a transpose operator; $x_{\min}$, $x_{\max}$, $y_{\min}$, and $y_{\max}$ represent the boundary of the work area, and $h_{\max}$ and $h_{\min}$ are the maximum and minimum permissible altitudes of the UAV, respectively. The maximum altitude of the UAV is affected by its size, weight, battery performance, and other characteristics. It can be restricted by regulations that are coordinated by agencies like the U.S. Federal Aviation Administration (FAA) [40].

2) DATA SLOT ALLOCATION PROBLEM

In this subsection, a data slot allocation problem is formulated regarding slot requests from the ground nodes. The UAV scheduler maximizes the level of satisfaction for all nodes under the concept of social welfare (SW), where the law of diminishing marginal utility [41] is applied. From this point of view, $U_i(s_i)$ represents node i's satisfaction according to

the number of assigned slots s_i, and $\sum U_i(s_i)$ is the total SW of this model:

$$U_i(s_i) = \log(Q_i(s_i) + 1)^{w_i}, \tag{5}$$

$$w_i = \gamma \cdot C'_{\text{group}}, \tag{6}$$

where weight factor $\gamma \in \{\gamma_1, \gamma_2\}$, and γ is set to γ_1 for real-time traffic and γ_2 for non-real-time traffic. C'_{group} is the group connectivity value in Eq. (3), assuming that only node i and its destination node are connected to the UAV. To assign slots to nodes, it is necessary to consider the following optimization problem.

Problem 2: Data Slot Allocation

$$\begin{aligned} &\max_{\boldsymbol{s}} \sum_{i \in \mathcal{N}} U_i(s_i) \\ &s.t. \quad C1 : \sum_{i \in \mathcal{N}} s_i \le T_s \\ &\qquad C2 : s_{\min_i} \le s_i \le r_i, \quad \forall_i \in \mathcal{N}, \end{aligned} \tag{7}$$

where $\boldsymbol{s} = [s_1, s_2, \ldots, s_N]^{\mathsf{T}}$, T_s, $s_{\min_i}$, and r_i are the total number of slots, the minimum number of slots, and the number of requested slots, respectively.

III. PROPOSED ALGORITHMS

A. UAV POSITIONING MECHANISM

We propose a solution to searching for the optimal position of the UAV. Each node exchanges its status and one-hop neighbor information, including its own position, in order to set up the network. Among the candidate positions for the UAV, the problem with 0 (a non-active link) or 1 (an active link) as a constraint in the optimization problem can be converted to binary integer linear programming (BILP), which can be solved using the branch-and-bound scheme [42] and the interior point method as a linear programming (LP) [43]. Then, we choose the minimum altitude, h, from among the feasible 3D positions for the UAV in order to enhance energy efficiency by refraining the UAV from being positioned at an unnecessarily high altitude. The proposed algorithm is explained in **Algorithm 1**.

In **Algorithm 1**, T_{clock} is the time clock of UAV. T_p is the UAV position update period. $x'_{\min}$ and $x'_{\max}$ are the minimum and maximum x value of all nodes, respectively. $y'_{\min}$ and $y'_{\max}$ are the minimum and maximum y value of all nodes, respectively.

In other studies involving commercial networks, since users are arbitrarily located around a base station, a UAV is positioned as high as possible in order to increase the coverage area. In a tactical MANET, however, since a MANET serves combatants with a plan, it is desirable to lower the altitude of the UAV as long as it successfully covers the network area, enhancing the survivability of the MANET. Moreover, this approach can minimize the energy consumption of the UAV when the nodes move to conduct tactical operations.

Algorithm 1 UAV Positioning Mechanism

Input : each node position, P_t
Return : UAV position (x^*, y^*, h^*)
While $T_{clock}/T_p = integer$
Do {
1: Solve $Loss_{max}$ between positions of node and UAV using TIREM, Rician, Rain Loss models.
2: Calculate P_r by solving (1).
3: Calculate C_{group} by solving (3).
4: Obtain feasible 3D positions by solving (4) using BILP with branch-and-bound method.
4-1: Find an optimal solution to LP model.
4-1-1: Reformulate (4) with updated possible position range C1, C2 of nodes and relaxed C4, C5.
$C1 : x'_{\min} \le x_u \le x'_{\max}$
$C2 : y'_{\min} \le y_u \le y'_{\max}$
$C3 : h_{\min} \le h_u \le h_{\max}$
$C4 : I_i \ge 0, i \in \mathcal{N}$
$C5 : G_j \ge 0, j \in \mathcal{M}$.
4-1-2: Apply reformulated (4) into the interior point method as LP in [43].
4-2: (At branch node 1)
UB (Upper Bound) = the relaxed solution;
LB (Lower Bound) = round-down solution;
4-3: Let R be the variable with the greatest fractional part for branching.
4-4: Create two new branch nodes for this variable,
(At branch node 2) R = 0;
(At branch node 3) R = 1;
4-5: (At branch node 2) Solve the reformulated (4) with R=0 using the LP model.
4-5-1: Apply reformulated (4) with R=0 into the interior point method as LP.
4-5-2: (At branch node 2)
UB (Upper Bound) = the relaxed solution;
LB (Lower Bound) = round-down solution;
4-6: The relaxed solution is the upper bound with R=0 using the LP model.
4-6-1: Apply reformulated (4) with R=1 into the interior point method as LP.
4-6-2: (At branch node 3)
UB (Upper Bound) = the relaxed solution;
LB (Lower Bound) = round-down solution;
4-7: **If** the process produces a feasible integer with the greatest upper bound value
then Save (x', y', h) as a feasible position.
If all variables are branched
then Return all feasible positions.
else Return to 4-3.
else Return to 4-3.
5: Choose the position with minimum h from among the feasible 3D positions.
}

Therefore, due to the differences in the purposes for serving these users, the biggest feature of the proposed algorithm compared to the conventional algorithm is that it considers connectivity between groups. Because it considers connectivity, it is not just the number of nodes to be connected, but process 3 in **Algorithm 1** that considers connectivity between groups according to topology. In addition, a difference compared to other algorithms is that the connectivity is obtained using topographic information, so it is process 1 in **Algorithm 1** where connectivity can be obtained more accurately. In order to prevent sudden changes in the UAV's position, we update the range of the UAV's position by limiting the range to the smallest value and the largest value among all previously known positions of all nodes from the initial operational range in process 4-1-1 of **Algorithm 1**.

B. DATA SLOT ALLOCATION MECHANISM

We present an optimal solution maximizing the QoS-based network utility.

Lemma 1: $U_i(s_i)$ is strictly concave.

Proof: From Eq. (5), we can write

$$U_i(s_i) = w_i \log(Q_i(s_i) + 1), \forall_i \in I,$$

where $w_i, Q_i(s_i), s_i > 0$.
For real-time $Q_i(s_i)$, utility concavity stems from:

$$\begin{aligned}\frac{d}{ds}Q_i(s_i) &= \frac{a_i c_i \exp(-a_i(s_i - b_i))}{(1 + \exp(-a_i(s_i - b_i))^2} > 0,\\ \frac{d^2}{ds^2}Q_i(s_i) &= -a_i^2 c_i \exp(-a_i(s_i - b_i))(1+ \exp(-a_i(s_i - b_i))^2\\ &\quad - 2a_i^2 c_i \exp(-2g_i(s_i - b_i))\\ &\quad \times (1 + \exp(-a_i(s_i - b_i))) < 0,\end{aligned}$$

and for non-real-time $Q_i(s_i)$:

$$\begin{aligned}\frac{d}{ds}Q_i(s_i) &= \frac{k_i}{(\log(1 + k_i s_{max}))(1 + k_i s_i)} > 0,\\ \frac{d^2}{ds^2}Q_i(s_i) &= \frac{-k_i^2}{(\log(1 + k_i s_{max}))(1 + k_i s_i)^2} < 0,\end{aligned}$$

resulting in

$$\begin{aligned}\frac{d}{ds}U_i(s_i) &= \frac{w_i Q_i(s_i)'}{Q_i(s_i) + 1} > 0,\\ \frac{d^2}{ds^2}U_i(s_i) &= -\frac{w_i Q_i(s_i)'^2}{(1 + Q_i(s_i))^2} + \frac{w_i Q_i(s_i)''}{(1 + Q_i(s_i))} < 0.\end{aligned}$$

Thus, $U_i(s_i)$ is strictly concave. □

Problem 2 becomes a standard convex optimization problem. A Lagrangian function for this convex optimization is given by

$$\begin{aligned}L(s, \boldsymbol{\pi}) = &\sum_{i\in I} w_i \log(U_i(s_i) + 1) - \lambda_1(\sum_{i\in I} s_i - T_s)\\ &+ \sum_{i\in I} \lambda_{2,i}(s_i - s_{\min_i}) - \sum_{i\in I} \lambda_{3,i}(s_i - r_i),\end{aligned} \tag{8}$$

where $\boldsymbol{\pi} = [\lambda_1, \boldsymbol{\lambda_2}^\intercal, \boldsymbol{\lambda_3}^\intercal]^\intercal$ is the updated Lagrange multiplier vector using the subgradient scheme [44]. We explain Lagrangian duality problem (8) as follows:

$$\min_{\boldsymbol{\pi}} \max_{s} L(\boldsymbol{s}, \boldsymbol{\pi}). \tag{9}$$

To find optimality in the Lagrangian duality problem, consider (9) as the problem associated with Lagrange multiplier vector $\boldsymbol{\pi}$. The duality theory allows the UAV to procure optimal slot allocation vector $\boldsymbol{s}^*(\boldsymbol{\pi})$ as follows:

$$\boldsymbol{s}^*(\boldsymbol{\pi}) = \arg \max_{\boldsymbol{s}} L(\boldsymbol{s}, \boldsymbol{\pi}). \tag{10}$$

By calculating iteratively, the dual variables vector can be obtained with:

$$\boldsymbol{\pi}(t) = \boldsymbol{\pi}(t-1) - \delta_\pi \frac{dL(\boldsymbol{s}, \boldsymbol{\pi})}{d\boldsymbol{\pi}}, \tag{11}$$

where δ_π is the positive and tiny step size that satisfies **Theorem 1** below. The uniqueness and optimality of the solution can be confirmed through an appropriate step size. The optimal solution will be obtained at the point where FONC is satisfied.

Theorem 1: If step size δ_π is chosen as $0 \le \delta_\pi \le \frac{2}{\tilde{\rho}\tilde{C}\tilde{R}}$ then sequence $(\boldsymbol{s}, \boldsymbol{\pi})$ converges to a point, $(\boldsymbol{s}^*, \boldsymbol{\pi}^*)$, and $\boldsymbol{s}^*$ is the only optimal solution to the problem.

Proof: Vector notations are used consistently in this Theorem. For vector $\boldsymbol{a} = (a_1, a_2, \ldots, a_n)^\intercal$, $||\boldsymbol{a}||_2$ is the Euclidean norm, $||\boldsymbol{a}||_1 = \sum_i |a_i|$, $||\boldsymbol{a}||_\infty = \max_i |a_i|$. In matrix $\boldsymbol{A}$, $||\boldsymbol{A}||$ is the induced norm.

We reformulate **Problem 2** as follows:

$$\begin{aligned}&\max_{\boldsymbol{s}} \sum_{i\in\mathcal{N}} U_i(s_i)\\ &s.t.\ \boldsymbol{As} \le \boldsymbol{c}\end{aligned} \tag{12}$$

where $2N + 1 \times N$ matrix

$$\boldsymbol{A} = \begin{bmatrix} 1 & 1 & 1 & \ldots & 1\\ 1 & 0 & 0 & \ldots & 0\\ 0 & 1 & 0 & \ldots & 0\\ . & & . & & \\ . & & & . & \\ 0 & & & & 1\\ -1 & 0 & 0 & \ldots & 0\\ 0 & -1 & 0 & \ldots & 0\\ . & & . & & \\ . & & & . & \\ 0 & & & & -1 \end{bmatrix},$$

$s = [s_1, s_2, \ldots, s_N]^\intercal$, and

$c = [T_s, r_1, r_2, \ldots, r_N, -s_{\min_1}, -s_{\min_2}, \ldots, -s_{\min_N}]^\intercal$.

The utility, $U_i(s_i)$, is non-negative, continuous, and strictly concave from **Lemma 1**. If step size δ_π is chosen appropriately small, the sequence $(\boldsymbol{s}, \boldsymbol{\pi})$ converges to point $(\boldsymbol{s}^*, \boldsymbol{\pi}^*)$, and $\boldsymbol{s}^*$ is the only optimal solution to the problem.

Let

$$\bar{C} = \max_{j\in\mathcal{N}} ||\boldsymbol{c}_{\_j}(A)||_1 \tag{13}$$

$$\bar{R} = \max_{i\in\{1,\cdots,2N+1\}} ||\boldsymbol{r}_{\_i}(A)||_1 \tag{14}$$

$$\frac{1}{\bar{\rho}} = \min_{i\in\mathcal{N}} \min_{s_{\min_i}\le s_i\le r_i} -U_i(s_i)'' > 0 \tag{15}$$

where $\boldsymbol{c}_{\_j}(A)$ and $\boldsymbol{r}_{\_i}(A)$ are the j-th column vector of $\boldsymbol{A}$ and the i-th row vector of $\boldsymbol{A}$, respectively, and $\bar{\rho}$ is the curvature radius of $U_i(s_i)$ in the range $[s_{\min_i}, r_i]$ [44]. $\mathcal{L}$ is a set of constraints, and $\mathcal{L}_i$ is a subset of $\mathcal{L}$ containing s_i in the constraints.

According to Lagrangian function (8), the dual objective function of optimization problem (12) is defined as follows:

$$D(\boldsymbol{\pi}) = \max_{\{s_{\min_i}\le s_i\le r_i|\forall i\in N\}} \left(\left(\sum_{i=1}^{N} [U_i(s_i) - s_i\pi^i] \right) + \sum_{l=1}^{2N+1} \pi_l c_l \right) \tag{16}$$

$$= \max_{\{s_{\min_i}\le s_i\le r_i|\forall i\in N\}} \sum_{i=1}^{N} \left(U_i(s_i(\pi^i)) - s_i\pi^i \right) + \sum_{l=1}^{2N+1} \pi_l c_l, \tag{17}$$

where

$$\pi^i = \sum_{l\in\mathcal{L}_i} \pi_l, \tag{18}$$

$$s_i(\pi^i) = [{U_i'}^{-1}(\pi^i)]_{s_{\min_i}}^{r_i}, \tag{19}$$

and $[z]_a^b = \min[\max(z, a), b]$ and ${U_i'}^{-1}$ is the inverse of U_i'.

Eq. (11) can be seen as a gradient projection to solve a dual problem.

$$D : \min_{\boldsymbol{\pi}\ge\mathbf{0}} D(\boldsymbol{\pi}). \tag{20}$$

Assumptions about the utility function are as follows:

A1: In the interval $I_i = [s_{\min_i}, r_i]$, utility function $U_i(s_i)$ is increasing, strictly concave, and twice continuously differentiable.

A2: The curvature of $U_i(s_i)$ is bounded away from zero on I_i: $-U_i''(s_i) \ge \frac{1}{\bar{\rho}_i} > 0$ for all $s_i \in F_i$

The following evidence is pertinent to Theorem 1 in [45].

Lemma 2: Dual function $D(\boldsymbol{\pi})$ is convex, lower bounded and continuously differentiable.

Proof: Let $B_i(\pi^i)$ be the first term of (20):

$$B_i(\pi^i) = \max_{s_i\in I_i} (U_i(s_i) - s_i\pi^i). \tag{21}$$

For $\pi^i \ge 0$, define $\beta_i(\pi^i)$ as

$$\beta_i(\pi^i) = \begin{cases} -\frac{1}{U_i''(s_i)}, & \text{if} \quad U_i'(r_i) \le \pi^i \le U_i'(s_{\min_i}) \\ 0, & \text{otherwise,} \end{cases}$$

where $s_i(\pi^i)$ is given as seen in (19), and is the unique maximizer of (21).

Let

$$\boldsymbol{B}(\boldsymbol{\pi}) = \text{diag}(\beta_i(\pi^i), i \in \mathcal{N}) \tag{22}$$

be an $N \times N$ diagonal matrix with diagonal elements $\beta_i(\pi^i)$. In assumption A2 for $\boldsymbol{\pi} \ge \mathbf{0}$,

$$0 \le \beta_i(\pi^i) \le \bar{\rho}_i < \infty. \tag{23}$$

Accordingly, all the diagonal elements are non-negative. □

Lemma 3: The Hessian of $D(\boldsymbol{\pi})$ is given by $H(D(\boldsymbol{\pi})) = \boldsymbol{A}\boldsymbol{B}(\boldsymbol{\pi})\boldsymbol{A}^\intercal$, where it exists.

Proof: Let $(\partial s/\partial\pi)(\boldsymbol{\pi})$ denote the $N\times(2N+1)$ Jacobian matrix for which the (i, l) element is $(\partial s_i/\partial\pi_l)(\boldsymbol{\pi})$. According to (19), $U_i'(s_i(\pi^i)) = \pi^i$, and $U_i''(s_i(\pi^i))(\partial s_i(\pi^i)/\partial\pi_i) = 1$, and therefore

$$\frac{\partial s_i}{\partial\pi_l}(\boldsymbol{\pi}) = \begin{cases} \dfrac{\boldsymbol{A}_{i,l}}{U_i''(s_i(\pi^i))}, & \text{if} \quad U_i'(r_i) \le \pi^i \le U_i'(s_{\min_i}), \\ 0, & \text{otherwise} \end{cases}$$

Using (22), we have the following.

$$\frac{\partial s}{\partial\pi}(\boldsymbol{\pi}) = -\boldsymbol{B}(\boldsymbol{\pi})\boldsymbol{A}^\intercal \tag{24}$$

Thus, from (17), we have $\nabla D(\boldsymbol{\pi}) = \boldsymbol{c} - \boldsymbol{A}\boldsymbol{s}(\boldsymbol{\pi})$, and therefore

$$H(D(\boldsymbol{\pi})) = -\boldsymbol{A}\left(\frac{\partial s}{\partial\pi}(\boldsymbol{\pi})\right) = \boldsymbol{A}\boldsymbol{B}(\boldsymbol{\pi})\boldsymbol{A}^\intercal. \tag{25}$$

□

Recall $\bar{C}$, $\bar{R}$, and $\bar{\rho}$ defined in (13)-(15), and we have the following lemma.

Lemma 4: $\nabla D(\boldsymbol{\pi})$ is Lipschitz with

$$||\nabla D(\boldsymbol{q}) - \nabla D(\boldsymbol{\pi})||_2 \le \bar{\rho}\bar{C}\bar{R}||\boldsymbol{q} - \boldsymbol{\pi}||_2 \tag{26}$$

for any vector $\boldsymbol{\pi}, \boldsymbol{q} \ge 0$.

Proof: Using **Lemma 3**, we will show that $||H(D(\boldsymbol{\pi}))||_2 = ||\boldsymbol{A}\boldsymbol{B}(\boldsymbol{\pi})\boldsymbol{A}^\intercal|| \le \bar{\rho}\bar{C}\bar{R}$.

With the definition of $\boldsymbol{B}(\boldsymbol{\pi})$ in (22),

$$||H(D(\boldsymbol{\pi}))||_2 = ||\boldsymbol{A}\boldsymbol{B}(\boldsymbol{\pi})\boldsymbol{A}^\intercal||_2 \tag{27}$$

$$\le \bar{\rho}||\boldsymbol{A}\boldsymbol{A}^\intercal||_2 \tag{28}$$

Since

$$||\boldsymbol{A}\boldsymbol{A}^\intercal||_2^2 \le ||\boldsymbol{A}\boldsymbol{A}^\intercal||_\infty ||\boldsymbol{A}\boldsymbol{A}^\intercal||_1$$

(as seen in [46], p.635) and $\boldsymbol{A}\boldsymbol{A}^\intercal$ is symmetric, $||\boldsymbol{A}\boldsymbol{A}^\intercal||_\infty = ||\boldsymbol{A}\boldsymbol{A}^\intercal||_1$, and hence

$$||\boldsymbol{A}\boldsymbol{A}^\intercal||_2 \le ||\boldsymbol{A}\boldsymbol{A}^\intercal||_\infty$$

$$= \max_l \textstyle\sum_{l'} [\boldsymbol{A}\boldsymbol{A}^\intercal]_{(l,l')}$$

$$= \max_l \textstyle\sum_{l'} \sum_i \boldsymbol{A}_{l,i}\boldsymbol{A}_{l',i}$$

$$\le \bar{C} \max_l \textstyle\sum_i \boldsymbol{A}_{l,i}$$

$$\le \bar{R}\bar{C}$$

With (28), we have a desirable (26).

□

Since $\boldsymbol{s}(\boldsymbol{\pi})$ in (19) is continuous, dual function $D(\boldsymbol{\pi})$ is lower bounded from **Lemma 2** and $\nabla D(\boldsymbol{\pi})$ is $\bar{\rho}\bar{C}\bar{R}$ Lipschitz from **Lemma 4**. Let $0 \le \delta_\pi \le \frac{2}{\bar{\rho}\bar{C}\bar{R}}$, and any random

sequence $\boldsymbol{\pi}(t)$ calculated by gradient projection algorithm (11) converges to the optimal point $\boldsymbol{\pi}^*$ of the dual problem. On the other hand, $\boldsymbol{s}^* = \boldsymbol{s}(\boldsymbol{\pi}^*)$ is the only solution for primal problem (12) (see [46], p.214). Therefore, the proof of **Theorem 1** is completed. □

Problem (9) can be solved by carrying out the Lagrangian dual method with the above analysis. The node workflow and the proposed scheme is shown in **Algorithm 2**. When the number of requested slots is smaller than the total available slots, the requested slots are allocated as requested. However, when the number of requested slots is greater than the total available slots, resources are allocated through the proposed algorithm. Basically, all nodes have the same opportunity, and can access the UAV. However, there are differences depending, on the traffic category. In the same traffic category, the ground nodes are treated fairly. However, importance of the traffic is the weight factor.

Algorithm 2 GC-TMAC Data Slot Allocation Mechanism

1: Send the number of slot requests, r_i, to the UAV.
2: Receive requested slots $\boldsymbol{s}$ from all nodes.
3: Check the sum of the requested slots with Total slot T_s
3-1: **if** $\sum_{i\in I} s_i \leq T_s$ **then**
  3-1-1: Choose slot allocation = requested slots and Return $\boldsymbol{s}$.
else
  3-2: Compute optimal data slot allocation using below process.
  3-2-1: Start with $\epsilon > 0$, $k = 0$ and input max iterations $K_{\max}$.
  3-2-2: Compute $L(\boldsymbol{s}, \boldsymbol{\pi}) = \sum_{i\in I} w_i \log(U_i(s_i) + 1) - \lambda_1(\sum_{i\in I} s_i - T_s) + \sum_{i\in I} \lambda_{2,i}(s_i - s_{\min_i}) - \sum_{i\in I} \lambda_{3,i}(s_i - r_i), \forall_i \in I$
  while
$$\max_{\boldsymbol{s}} \frac{dL(\boldsymbol{s}, \boldsymbol{\pi})}{d\boldsymbol{\pi}} \geq \epsilon$$
  do
    if $k < K_{\max}$ **then**
      Solve (9) and obtain $\boldsymbol{s}^k$
      Update $\boldsymbol{\pi}^{k+1}$; Set $k \leftarrow k + 1$;
    else
      return $\boldsymbol{s}^k$
  and Return $\boldsymbol{s}$.
4: Release slot assignment s_i of node i for each node.

Table 2 illustrates both conventional- and proposed-algorithm complexity. In **Problem 1**, the branch and bound strategy is used to solve optimization problems without a conventional exhaustive search method in the average case. In order to avoid an $n!$ exhaustive search, the branch and bound method takes $O(\log_2 n)$ searches on average [47]. In **Problem 2**, the gradient descent method is used to solve the maximization problem.

In the proposed system, it is a requirement that nodes with mobility form various groups and send various types of traffic. In this situation, the demand for communication through the UAV is high, so a resource allocation method in the UAV is required. Therefore, the proposed algorithm is different from the existing algorithm that simply allocates slots proportionally when there are more slots required than available slot resources. That can occur in a situation where the demand to transmit data through the UAV is high. The biggest feature is process 3-2 in **Algorithm 2** that allocates slot resources based on characteristics.

TABLE 2. Algorithm Computational Complexity.

	Conventional	Proposed
Problem 1	$\mathcal{O}(n!)$	$\mathcal{O}(\log_2 n))$
Problem 2	$\mathcal{O}(n^3)$	$\mathcal{O}(n^2)$

The computational cost of gradient descent depends on the number of iterations it takes to converge. Compared to the complexity of the closed form of linear regression, $O(n^3)$, the complexity of gradient descent $O(n^2)$ is low [48]. Hence, when n is very large, it is recommended to use gradient descent instead of the closed form of linear regression.

IV. NUMERICAL RESULTS

Numerical results verify the effectiveness of the proposed algorithm using Riverbed Modeler 18.6 [49]. Also, the Unity 3D visualization tool and the Simulation Monitoring Analysis Tool (SMAT) [50] are used to represent a 3D image through a linkage with the Riverbed Modeler. TIREM-4 and Rician fading distribution models were applied to 14 km by 14 km mountain and plain areas to configure channels similar to tactical fields. For the mountain and plain areas, Cheorwon, Gangwon-do province (center coordinates latitude N38.108136, longitude E127.1423) and the city of Paju (center coordinates latitude N37.8697, longitude E126.747) in South Korea were chosen. Moreover, DTED-2 was applied to these areas, as shown in Fig. 7. The system parameters are summarized in Table 3, which can be set differently depending on the operating environment. A single node is connected to another node when the received signal power is higher than the minimum received power level. This is the design value of our radio system, which is −78 dBm as shown in Table 3. We assume that the maximum number of nodes that can be assigned a slot in the same superframe is 24 and, as long as any two nodes are linked within 4-hops, they can communicate with each other through ad-hoc networking and all nodes within 4 km and in the same group can communicate with each other.

In Figs. 8-9 for the first scenario, the system had three operational groups: Group 1 with 20 nodes, Group 2 with 15 nodes, and Group 3 with five nodes. In this scenario, those three operational groups initially stood at the same starting point. Then, Group 1 remained stationary, and Group 2 and Group 3 started to move in different directions. When the three groups are stationed closely, they can communicate with each other as a single network. However, when the groups are separated widely, they are not fully connected in an ad-hoc mode. They are separated into different groups, and a UAV can connect those groups.

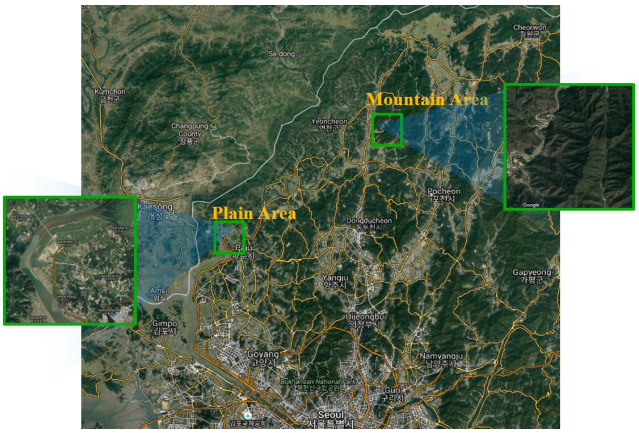

FIGURE 7. **Link budget analysis target areas - mountain area: Cheorwon, Gangwon-do province in South Korea (center coordinates latitude N38.108136, longitude E127.1423), and the plain area: Paju in South Korea (center coordinates latitude N37.8697, longitude E126.747).**

TABLE 3. **System Parameters.**

Parameters	Values
Frequency	700 MHz
Bandwidth	8 MHz
Physical data rate	4 Mbps
UAV position update period, T_p	5 minutes
Ground node maneuvering speed	6 km/h
Link budget loss model	Channel models in Table 1
Rician factor, K	15 dB
Availability for Rician fading	99%
Rician fading margin	4.7605 dB
Rain fading	0 dB
Transmit power (EIRP), P_t	26 dBm
Received power threshold, P_{th}	-78 dBm
UAV altitudes, $h_{\min}, h_{\max}$	100 m, 1000 m
QoS parameters, a_i, b_i, k_i, s_{max}	10 / 1 / 30 / 100
Connectivity parameter, α, β	0.1 / 10
Traffic weight factor, γ_1, γ_2	1.5 / 1
Minimum slots for nodes, $s_{\min}$	0
Slot requests for nodes, $r_{i_{real}}$, $r_{i_{non-real}}$	4 / 10
Superframe size	100 ms
Duration of a slot	1 ms
Total data slots	48
Maximum iteration number, $K_{\max}$	100

Figure 8 shows the positions at the starting point. The blue text and blue circle represent the position of the UAV as calculated by a conventional algorithm, Drone Based Station (DBS) [10], where the UAV is stationed at the center of the whole group at its maximum altitude (1000 m). The conventional algorithm tries to increase the altitude of the UAV until it attains maximum coverage. Conversely, the red text and red circle from the proposed scheme show that the UAV position is at the center of the whole group, and its altitude at the starting point is at the minimum (100 m). With the nodes concentrated around the starting point, the UAV tries to decrease its altitude to as low as possible while still covering all nodes.

In a single group, the nodes are fully connected, i.e., node connectivity is guaranteed without support from the UAV. In this case, the UAV can be used to increase QoS, such as

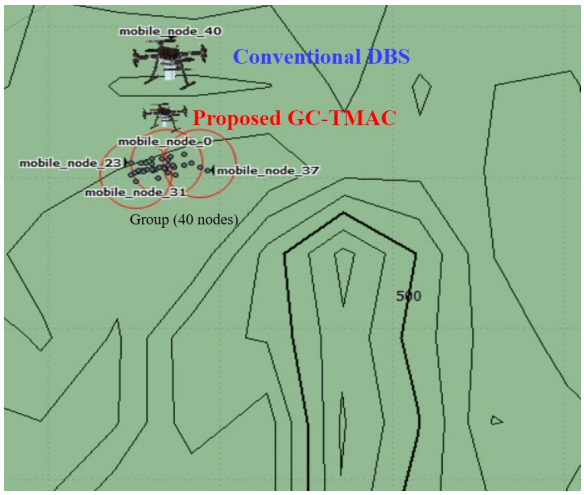

(a) UAV position comparison in a single network group

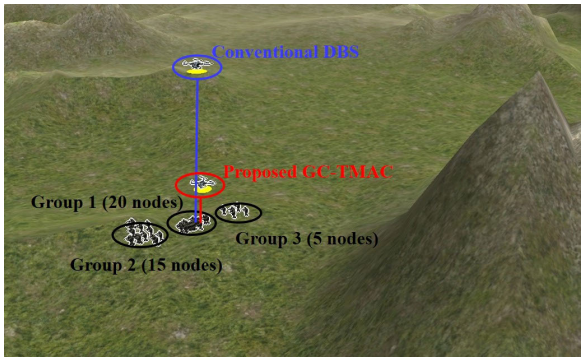

(b) SMAT 3D-image of UAV position comparison in a single network group

FIGURE 8. **UAV position comparison in a single network group for a target mountain area.**

delay minimization, by providing alternative paths to connect the nodes. However, when more than two groups exist, inter-group connectivity can be supported with the UAV relaying data.

Figure 9 shows the results when the groups move in different directions. The blue text and circle indicate the UAV's position under the conventional algorithm when two groups move in different directions. The conventional algorithm considers the maximum coverage and number of user nodes. It increases the altitude of the UAV until its coverage increases. If it reaches the maximum altitude, it finds a horizontal position for the UAV that covers the maximum number of nodes. In figures 9 (a) and (b), the UAV is stationed where it can support all the nodes of Group 1 and Group 2, even though it cannot support the five nodes of Group 3 at all. On the other hand, the proposed scheme considers not only the number of nodes but also the number of groups, and this is the main difference from the conventional algorithm. The proposed scheme places the UAV to maximize group connectivity. Then, it decreases the altitude of the UAV to as low as possible while maximum group connectivity is still guaranteed. In this figure, the UAV is stationed where it can support all three groups, but the supported number of nodes

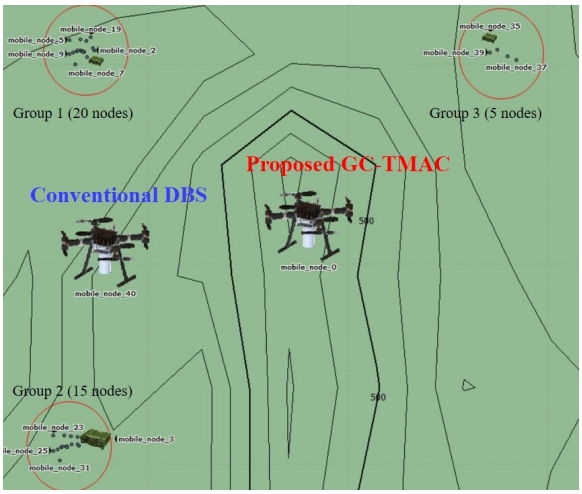

(a) UAV position comparison for network's three groups

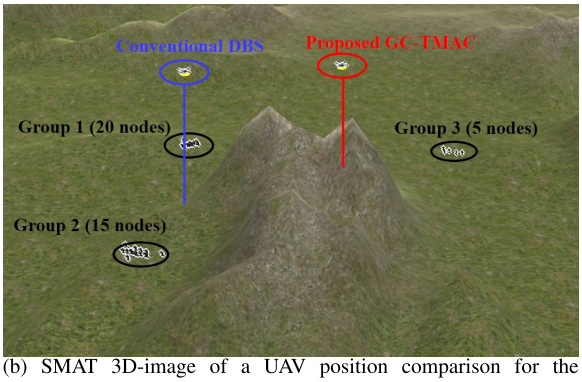

(b) SMAT 3D-image of a UAV position comparison for the network's three groups

FIGURE 9. UAV position comparison for the network's three groups in a mountain area.

is two nodes in Group 1, one node in Group 2, and a single node in Group 3. Although the number of nodes linked by the proposed algorithm is less than the conventional algorithm, it has better group connectivity.

Figure 10 (a) is a comparison between the conventional algorithm and the proposed algorithm for the number of nodes linked to the UAV as the groups move on the plain area (light blue and blue bar) and on the mountain area(purple and red bar). When the distance of the group increases to some extent, the existing algorithm moves the UAV to maximize the number of connected nodes. However, since the proposed algorithm also increases group connectivity, the number of nodes linked to the UAV (an average of 15.25 nodes) is lower than with the conventional algorithm (an average of 27 nodes).

Figure 10 (b) shows the group connectivity between the conventional algorithm and the proposed algorithm as the groups move on the plain area and on the mountain area. Since the proposed algorithm locates the UAV to maximize connection of the inter-group rather than the sum of the connections, group connectivity under the proposed algorithm is higher than the conventional algorithm, unlike the results in Figure 10 (a). The average for group connectivity with the proposed algorithm is 26.525, while that of the conventional algorithm is 17.7.

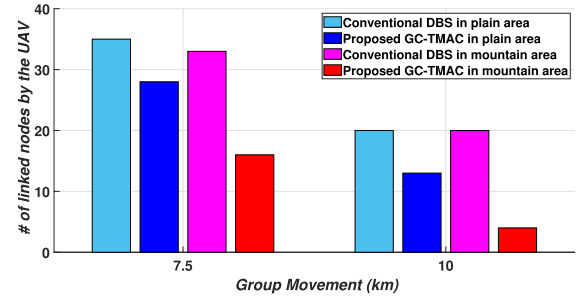

(a) Number of nodes linked to the UAV

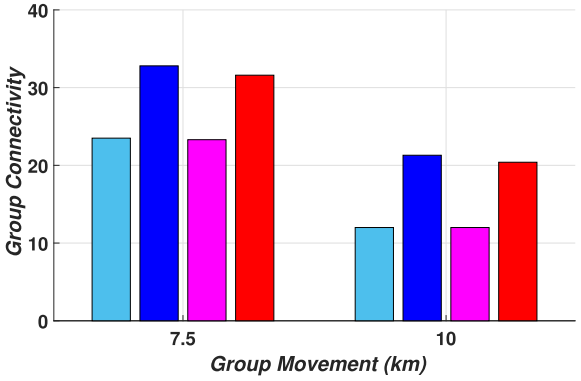

(b) Group connectivity

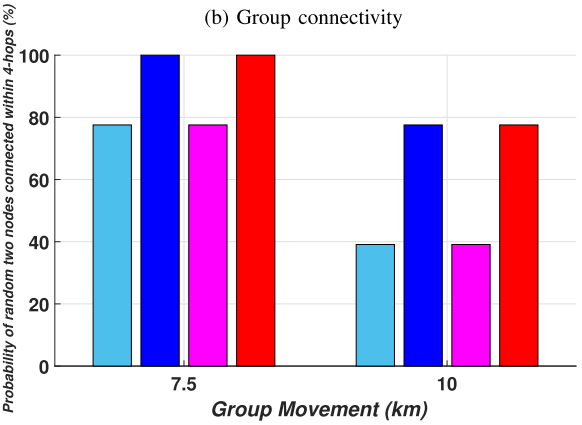

(c) Probability of two random nodes connected within four-hops

FIGURE 10. Comparison based on group movement.

Figure 10 (c) is a comparison of the probability of two randomly selected nodes being connected within four-hops. Note the assumption that any two nodes linked within four-hops can communicate with each other through ad-hoc networking. The probability under the proposed algorithm (88.78%) is higher than under the conventional algorithm (58.33%).

Figure 11 shows the group connectivity between the conventional algorithm and the proposed algorithm as the groups move on the plain and in the mountain area based on movement time. Up to about 50 minutes, all four graphs have the same value, because all nodes and all groups are covered. However, a difference appears after about 55 minutes, and the GC value starts to become small because the conventional method moves the UAV in a direction increasing the number of nodes. In contrast, the proposed GC-TMAC maintains a relatively high GC value. In order to show robustness, the location of the UAV is updated every 5 minutes, and we

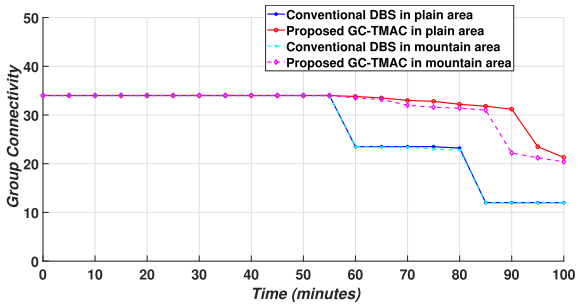

FIGURE 11. Group Connectivity according to time (minutes).

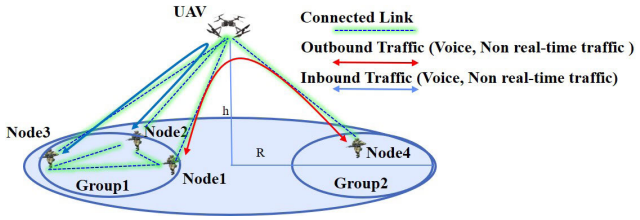

FIGURE 12. Scenario for slot allocation.

confirmed that the UAV does not suddenly deviate from the range of the nodes.

The second scenario is shown in Figure 12. The two divided groups are all connected to the UAV. Node 1 of Group 1 transmits one voice traffic and one non-real-time outbound traffic to Node 4 of Group 2 via the UAV. Node 2 and Node 3 of Group 1 transmit inbound one voice traffic and one non-real-time traffic within the same group via the UAV. Then, the total number of nodes was increased to 20 nodes from four nodes in increments of four nodes; With each increment, three nodes were added to for Group 1 and one node was added to Group 2.

In Figure 13, the allocated data slots under the proposed algorithm, with and without a GC value, are compared with K-Desync [16] and W-Desync [16] as the conventional algorithms. The proposed without-GC algorithm means that w_i in Eq. (5) is fixed at 1. The proposed without-GC algorithm is added in the comparative analysis to verify the effect of GC in the scheduling. Since the proposed GC-TMAC algorithm considers inter-group connectivity and real-time traffic more important, as shown in Eq. (5), the group connectivity and QoS satisfaction are reflected as weight factors in the GC utility. Accordingly, if the available slots are insufficient to meet the requests, the slots are assigned preferentially to outbound traffic, rather than inbound traffic, and to real-time traffic rather than non-real-time traffic. However, because the proposed without-GC algorithm does not consider group connectivity, it preferentially assigns slots to real-time traffic, rather than non-real-time traffic. K-Desync [16] allocates slots evenly to all nodes when slots are insufficient, whereas W-Desync allocates slots according to weigh factor z; that is, the number of nodes requested slot. This characteristic is confirmed from the following the four results in Figure 13.

Figure 13 (a) is the result for outbound voice traffic. As the number of nodes increases, the proposed GC-TMAC algorithm increases the slot allocations, even when the number of available slots is less than the required slots, by rescheduling the total number of slots. Also, the proposed without-GC algorithm increases slot allocation due to the fast increment of QoS satisfaction for real-time traffic. However, the conventional algorithms do not allocate additional slots after a certain number of nodes.

Figure 13 (b) is the result for non-real-time outbound traffic. As the number of nodes increases, the proposed GC-TMAC algorithm increases the slot allocations. However, the conventional algorithms do not allocate additional slots. When the total number of nodes is more than 16, the proposed GC-TMAC algorithm decreases slot allocations to non-real-time outbound traffic, because the slots for voice outbound traffic are preferentially allocated when the number of slots is insufficient. The proposed without-GC algorithm does not allocate slots because it does not consider the weight of group connectivity, and it does not prefer non-real-time traffic.

Figure 13 (c) shows the result for inbound voice traffic. As the number of nodes increases, the proposed GC-TMAC algorithm increases the slot allocations, and then, the number of slots for the proposed GC-TMAC decreases in order to preferentially allocate the requested slots to outbound traffic. However, in the conventional methods, when the number of nodes increases, if the total number of slots becomes insufficient, additional allocations to outbound traffic is not possible. The proposed without-GC algorithm, however, allocates slots since it prefers non-real-time traffic without considering the weight of group connectivity.

Figure 13 (d) shows slot allocation for non-real-time inbound traffic. Overall, it shows that the proposed GC-TMAC algorithm assigns a low number of slots. The conventional methods further cannot increase data slot allocation for the more important traffic as the number of nodes increases, because the non-real-time inbound traffic already occupies a considerable number of slots. However, under the proposed GC-TMAC, if the number of nodes is eight or more, slots are not allocated to non-real-time inbound traffic, because it has the lowest priority, whereas the proposed without-GC algorithm shows the same results as shown in Figure 12 (b) because it does not distinguish inbound traffic from outbound traffic.

Overall, the conventional methods cannot increase data slots as the number of nodes increases and the total number of slots becomes insufficient. The proposed without-GC algorithm allocates slots preferentially to real-time traffic. However, in the proposed GC-TMAC algorithm, when the total number of slots is insufficient, allocation to outbound traffic can be further increased by decreasing slots allocated to inbound traffic. When the number of available slots becomes insufficient for inbound traffic, slots are assigned to voice traffic between the groups, because this real-time traffic is more important than non-real-time traffic.

Figure 14 shows the ratio of the allocated slots to the requested slots for each type of traffic. In the conventional K-Desync, as it allocates slots evenly to the nodes regardless

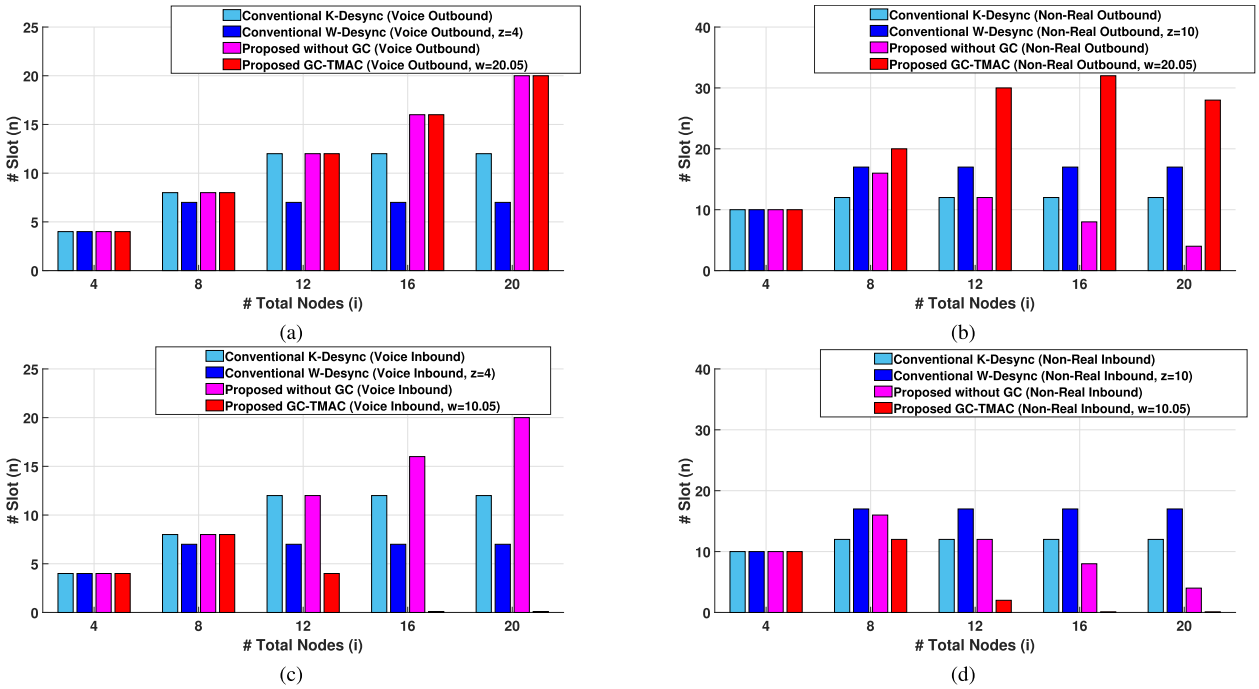

FIGURE 13. Allocated data slots comparison (a) voice outbound traffic (b) non-real-time outbound traffic (c) voice inbound traffic (d) non-real-time inbound traffic.

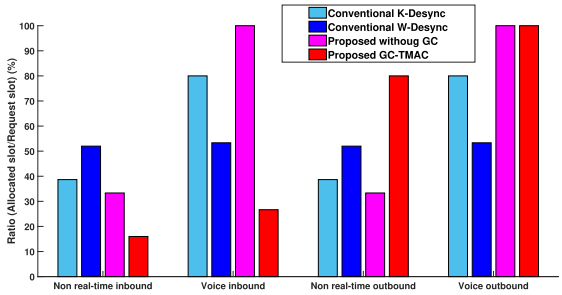

FIGURE 14. Allocated data ratio comparison for in/outbound, non-real-time/real-time traffic.

of requested slots, it shows a high ratio of voice traffic, which has a relatively low number of requested slots. In the conventional W-Desync, there is little difference in the ratio for each type of traffic because it allocates slots in proportion to requests. The proposed without-GC algorithm, only allocates more slots to real-time traffic. However, the proposed GC-TMAC algorithm allocates slots by reflecting different levels of group connectivity according to the type and direction of the traffic.

V. CONCLUSION

In this paper, we investigated a UAV positioning problem for GC maximization, and a data slot-allocation problem for GC utility maximization. Then, we proposed an optimal positioning and slot allocation mechanisms providing for the priorities of the groups and the traffic in a tactical MANET. Through these algorithms, the UAV is positioned to maximize GC rather than the number of nodes. The traffic designated to another group or carrying real-time voice is assigned slots preferentially. In the numerical analysis, the results verify the effectiveness of the proposed scheme in UAV positioning and data slot allocation. As future work, we will verify GC-TMAC in more varied topologies, and will research where to place each UAV when there are multiple UAVs as to which location can maximize survivability and connectivity, and we will improve communication performance through collaboration relays between UAVs.

REFERENCES

[1] J. S. Lee, Y.-S. Yoo, H. S. Choi, and J. K. Choi, "Energy-efficient TDMA scheduling for UVS tactical MANET," *IEEE Commun. Lett.*, vol. 23, no. 11, pp. 2126–2129, Nov. 2019.

[2] I. Bor-Yaliniz and H. Yanikomeroglu, "The new frontier in RAN heterogeneity: Multi-tier drone-cells," *IEEE Commun. Mag.*, vol. 54, no. 11, pp. 48–55, Nov. 2016.

[3] M. Alzenad, A. El-Keyi, F. Lagum, and H. Yanikomeroglu, "3-D placement of an unmanned aerial vehicle base station (UAV-BS) for energy-efficient maximal coverage," *IEEE Wireless Commun. Lett.*, vol. 6, no. 4, pp. 434–437, Aug. 2017.

[4] L. Zhang and N. Ansari, "On the number and 3-D placement of in-band full-duplex enabled drone-mounted base-stations," *IEEE Wireless Commun. Lett.*, vol. 8, no. 1, pp. 221–224, Feb. 2019.

[5] A. Al-Hourani, S. Kandeepan, and S. Lardner, "Optimal LAP altitude for maximum coverage," *IEEE Wireless Commun. Lett.*, vol. 3, no. 6, pp. 569–572, Dec. 2014.

[6] V. Sharma, M. Bennis, and R. Kumar, "UAV-assisted heterogeneous networks for capacity enhancement," *IEEE Commun. Lett.*, vol. 20, no. 6, pp. 1207–1210, Jun. 2016.

[7] M. Mozaffari, W. Saad, M. Bennis, and M. Debbah, "Efficient deployment of multiple unmanned aerial vehicles for optimal wireless coverage," *IEEE Commun. Lett.*, vol. 20, no. 8, pp. 1647–1650, Aug. 2016.

[8] Y. Chen, W. Feng, and G. Zheng, "Optimum placement of UAV as relays," *IEEE Commun. Lett.*, vol. 22, no. 2, pp. 248–251, Feb. 2018.

[9] X. Sun and N. Ansari, "Latency aware drone base station placement in heterogeneous networks," in *Proc. IEEE Global Commun. Conf.*, Dec. 2017, pp. 1–6.

[10] M. Alzenad, A. El-Keyi, and H. Yanikomeroglu, "3-D placement of an unmanned aerial vehicle base station for maximum coverage of users with different QoS requirements," *IEEE Wireless Commun. Lett.*, vol. 7, no. 1, pp. 38–41, Feb. 2018.

[11] S. Goyal, P. Liu, and S. S. Panwar, "User selection and power allocation in full-duplex multicell networks," *IEEE Trans. Veh. Technol.*, vol. 66, no. 3, pp. 2408–2422, Mar. 2017.

[12] A. Sgora, D. J. Vergados, and D. D. Vergados, "A survey of TDMA scheduling schemes in wireless multihop networks," *ACM Comput. Surv.*, vol. 47, no. 3, p. 53, 2015.

[13] T. Kaur and D. Kumar, "TDMA-based MAC protocols for wireless sensor networks: A survey and comparative analysis," in *Proc. 5th Int. Conf. Wireless Netw. Embedded Syst. (WECON)*, Oct. 2016, pp. 1–6.

[14] Harris. *FALCON IIIâ RF-7800V-HH*. Accessed: 2020. [Online]. Available: https://www.harris.com/sites/default/les/rf-7800v-hh-handheld-vhftactical-combat-net-radio.pdf

[15] J.-Y. Jung, H.-H. Choi, and J.-R. Lee, "Survey of bio-inspired resource allocation algorithms and MAC protocol design based on a bio-inspired algorithm for mobile ad hoc networks," *IEEE Commun. Mag.*, vol. 56, no. 1, pp. 119–127, Jan. 2018.

[16] U. Yu, H. Choi and J. Lee, "Kuramoto-desync: Distributed and fair resource allocation in a wireless network," *IEEE Access*, vol. 7, pp. 104769–104776, 2019.

[17] U.-S. Yu, J.-Y. Jung, E. Kong, H. Choi, and J.-R. Lee, "Weighted-DESYNC and its application to end-to-end throughput fairness in wireless multihop network," *Mobile Inf. Syst.*, vol. 2017, Apr. 2017, Art. no. 2504604.

[18] J.-R. Cha, K.-C. Go, J.-H. Kim, and W.-C. Park, "TDMA-based multi-hop resource reservation protocol for real-time applications in tactical mobile adhoc network," in *Proc. Mil. Commun. Conf.*, Oct. 2010, pp. 1936–1941

[19] C. Zhu and M. S. Corson, "An evolutionary-TDMA scheduling protocol(E-TDMA) for mobile ad hoc networks," in *Proc. ATIRP*, 2000.

[20] P. Djukic and S. Valaee, "Distributed link scheduling for TDMA mesh networks," in *Proc. IEEE Int. Conf. Commun.*, Jun. 2007, pp. 3823–3828.

[21] A. Sayadi, B. Wehbi, and A. Laouiti, "One shot slot TDMA-based reservation MAC protocol for wireless ad hoc networks," in *Proc. IEEE 73rd Veh. Technol. Conf.*, May 2011, pp. 1–5.

[22] A. Kanzaki, T. Uemukai, T. Hara, and S. Nishio, "Dynamic TDMA slot assignment in ad hoc networks," in *Proc. 17th Int. Conf. Adv. Inf. Netw. Appl.*, 2003, pp. 330–335.

[23] C. Zhu and M. S. Corson, "A five-phase reservation protocol (FPRP) for mobile ad hoc networks," in *Proc. 17th Annu. Joint Conf. IEEE Comput. Commun. Soc.*, Dec. 1998.

[24] I. Rhee, A. Warrier, J. Min, and L. Xu, "DRAND: Distributed randomized TDMA scheduling for wireless ad hoc networks," *IEEE Trans. Mobile Comput.*, vol. 8, no. 10, pp. 1384–1396, Dec. 2009.

[25] Y. Wang and I. Henning, "A deterministic distributed TDMA scheduling algorithm for wireless sensor networks," in *Proc. Int. Conf. Wireless Commun., Netw. Mobile Comput.*, Sep. 2007, pp. 2759–2762.

[26] W. Khawaja, I. Guvenc, D. Matolak, U.-C. Fiebig, and N. Schneckenberger, "A survey of Air-to-Ground propagation channel modeling for unmanned aerial vehicles," 2018, *arXiv:1801.01656*. [Online]. Available: http://arxiv.org/abs/1801.01656

[27] *Examples of Technical Characteristics for Unmanned Aircraft Control and Non-Payload Communications Links*, document ITU-R M.2233, Nov. 2011.

[28] *ABSOLUTE—Aerial Base Stations with Opportunistic Links for Unexpected & Temporary Events*, document RP7-ICT-2011-8-318632-ABSOLUTE/D2.3, Oct. 2013.

[29] A. Zavala, J. Ruiz, and J. Penin, *High-Altitude Platforms for Wireless Communications*. Hoboken, NJ, USA: Wiley, 2008.

[30] *VHF Air-Ground and Air-Air Digital Link (VDL) Mode 4 Radio Equipment: Technical Characteristics and Methods of Measurement for Aeronautical Mobile (Airborne) Equipment: Part 1: Physical Layer*, document ETSI EN 302 842-1, Oct. 2011.

[31] *Public Mobile Telecommunication Service With Aircraft Using the Bands 1 800-1 805 MHz*, document ITU-R M.1040 1994.

[32] *US Department of Defense, Electromagnetic Compatibility Analysis Center*, document ECAC-HDBK-93-076, Jul. 1995. [Online]. Available: https://apps.dtic.mil/docs/citations/ADA296913

[33] *Performance Specification Digital Terrain Elevation Data (DTED)*, document US MIL-RPRF-89020B, May 2000.

[34] A. A. Khuwaja, Y. Chen, N. Zhao, M. S. alouni, and P. Dobbins, "A survery of channel modeling for UAV communications," *IEEE Commun. Surveys Tuts.*, vol. 20, no. 4, pp. 2804–2821, 4th Quart., 2018.

[35] D. W. Matolak and R. Sun, "Air–Ground channel characterization for unmanned aircraft Systems—Part I: Methods, measurements, and models for over-water settings," *IEEE Trans. Veh. Technol.*, vol. 66, no. 1, pp. 26–44, Jan. 2017.

[36] *Progagation Data and Prediction Methods Requred for the Design of Earth Space Telecommunication Systems*, document ITU-R P.618-13 2017.

[37] Y. Wang and A. Abdelhadi, "A QoS-based power allocation for cellular users with different modulations," in *Proc. Int. Conf. Comput., Netw. Commun. (ICNC)*, Feb. 2016, pp. 19–24.

[38] *Analog to Digital Conversion of Voice by 2,400 Bit/Second Mixed Excitation Linear Prediction (MELP)*, document US DoD MIL. STD. 3005, 2005.

[39] A. Abdel-Hadi and C. Clancy, "A utility proportional fairness approach for resource allocation in 4G-LTE," in *Proc. Int. Conf. Comput., Netw. Commun. (ICNC)*, Feb. 2014, pp. 1034–1040, doi: 10.1109/ICCNC.2014.6785480.

[40] *Drones in Canada*. Accessed: 2020. [Online]. Available: https://www.priv.gc.ca/en/opc-actions-and-decisions/research/explore-privacy-research/2013/dronds-201303/

[41] M. C. Rios, C. R. McConnell, and S. L. Brue, *Economics: Principles, Problems, and Policies*. New York, NY, USA: McGraw-Hill, 2004.

[42] Y. Shi and H. Lee, *A Binary Integer Linear Program With Multi Criteria and Multi-Constraint Levels*. Amsterdam, The Netherlands: Elsevier, 1997.

[43] A. S. Nemirovski and M. J. Todd, "Interior-point methods for optimization," *Act, Num.*, vol. 17, 191–234, Aug. 2008.

[44] S. Boyd and L. Vandenberghe, *Convex Optimization*. New York, NY, USA: Cambridge Univ. Press, 2004.

[45] W. H. Wang, M Palaniswami and H. Low, "Application-oriented flow control: Fundamentals, algorithims and fairness," *IEEE/ACM Trans. Netw.*, vol. 14, no. 6, pp. 1282–1291, Dec. 2006.

[46] D. Bertsekas and J. N. Tsitsiklis, *Parallel and Distributed Computation*. Englewood Cliffs, NJ, USA: Prentice-Hall, 1997.

[47] J. Herrera, J. Salmerãn, and E. Hendrix, "On parallel branch and bound frameworks for global optimization," *J. Global Optim.*, vol. 69, pp. 547–560, Nov. 2017.

[48] *Machine Learning course by Stanford University*. Accessed: 2020. [Online]. Available: https://www.coursera.org/learn/machine-learning/supplement/bjjZW/normal-equation

[49] *Riverbed Modeler 18.6*. Accessed: 2020. [Online]. Available: https://support.riverbed.com/content/support/software/steelcentral-npm/modeler-index.html?swVersion=18.6.0

[50] *Unity Simulation Monitoring Analysis Tool*. Accessed: 2020. [Online]. Available: https://unity.com/solutions

JAE SEANG LEE (Member, IEEE) received the B.S. degree in electrical engineering from Korea University, Seoul, South Korea, in 2006, and the M.S. degree in electrical engineering from the Korea Advanced Institute of Science and Technology (KAIST), Daejeon, South Korea, in 2008, where he is currently pursuing the Ph.D. degree in electrical engineering. He is currently a Senior Researcher with the 2nd Research Department, Agency for Defense Development (ADD), Daejeon. His research interests include tactical mobile ad-hoc networks and network optimization.

YOON-SIK YOO (Member, IEEE) received the B.S. and M.S. degrees in electronic engineering from Sungkyunkwan University, Suwon, Republic of Korea, in 1999 and 2001, respectively, and the Ph.D. degree from the School of Electrical Engineering, Korea Advanced Institute of Science and Technology (KAIST), Daejeon, Republic of Korea, in 2020. He joined the Electronics and Telecommunications Research Institute (ETRI), in 2001. He is currently working as a Principal Researcher with the Energy ICT Research Section. Since 2001, he has developed home network management agent, context-aware intelligent agent, wireless LAN platform and ubiquitous service framework, smart grid, energy management systems, virtual power plant (VPP) systems, and energy trading systems. His current research interests include demand-side energy management optimization, demand-supply energy balancing, distributed energy resources (DERs) management technology, and energy broker mechanism for small-scale DERs. He received the Excellent Paper Award at the Telecommunications Technology Association (TTA), in 2008. Recently in 2019, he won the Excellent Researcher Award in ETRI.

HYUNGSEOK CHOI received the B.S. and M.S. degrees in electrical engineering from Korea University, South Korea, in 1998 and 2002, respectively, and the Ph.D. degree in electrical engineering from Chungnam National University, Daejeon, South Korea, in 2014. He joined the Agency for Defense Development (ADD), in 2002, where he is currently a Principle Researcher. His research interests include military communication satellite systems and tactical information communications network systems.

TAEJOON KIM (Member, IEEE) received the B.S. degree in electronics engineering from Yonsei University, Seoul, South Korea, in 2003, and the Ph.D. degree in electrical engineering from the Korea Advanced Institute of Science and Technology, Daejeon, South Korea, in 2011. From 2003 to 2005, he was a Researcher with LG Electronics, Seoul. From 2011 to 2013, he was a Senior Researcher with the Electronics and Telecommunications Research Institute, Daejeon. He is currently an Associate Professor with the School of Information and Communication Engineering, Chungbuk National University, Chungju, South Korea. His research interests include communication theory and analysis and optimization of wireless networks.

JUN KYUN CHOI (Senior Member, IEEE) received the B.Sc. (Eng.) degree in electronics engineering from Seoul National University, Seoul, South Korea, in 1982, and the M.Sc. (Eng.) and Ph.D. degrees in electronics engineering from the Korea Advanced Institute of Science and Technology (KAIST), Daejeon, South Korea, in 1985 and 1988, respectively. From June 1986 to December 1997, he was with the Electronics and Telecommunication Research Institute. In January 1998, he joined Information and Communications University, Daejeon, as a Professor. In 2009, he moved to KAIST as a Professor. He is an Executive Member of the Institute of Electronics Engineers of Korea, a member of the Editorial Board for the Korea Information Processing Society, and a Life Member of the Korea Institute of Communication Science.